IJRCS

International Journal of Robotics and Control Systems
Vol. 5, No. 2, 2025, pp. 902-916
ISSN 2775-2658
http://pubs2.ascee.org/index.php/ijrcs

ASCEE

Optimization of Harmonic Elimination in PV-Fed Asymmetric Multilevel Inverters Using Evolutionary Algorithms

Taha Abdulsalam Almalaisi [a,b,1], Noor Izzri Abdul Wahab [a,2], Hussein I. Zaynal [c,3,*], Mohd Khair Hassan [a,4], Hasan S. Majdi [d,5], Ahmed Dheyaa Radhi [e,6], Nitin Solke [f,7], Ravi Sekhar [f,8]

[a] Department of Electrical and Electronics Engineering, University Putra Malaysia (UPM), Serdang, Selangor 43400, Malaysia
[b] Unit of Renewable Energy, Northern Technical University, Kirkuk, Iraq
[c] Department of Computer Engineering Technology, Al-Kitab University, Altun Kupri, Iraq
[d] Department of Chemical Engineering and Petroleum Industries, Al-Mustaqbal University College, 51001 Hillah, Babylon, Iraq
[e] College of Pharmacy, University of Al-Ameed, Karbala PO Box 198, Iraq
[f] Symbiosis Institute of Technology (SIT) Pune Campus, Symbiosis International (Deemed University) (SIU), Pune, 412115, Maharashtra, India
[1] gs63720@student.upm.edu.my; [2] izzri@upm.edu.my; [3] drhussain.i.zainal@gmail.com; [4] khair@upm.edu.my;
[5] dr.hasanshker@mustaqbal-college.edu.iq; [6] ahmosawi@alameed.edu.iq; [7] nitin.solke@sitpune.edu.in;
[8] ravi.sekhar@sitpune.edu.in
* Corresponding Author

ARTICLE INFO

Article history
Received January 28, 2025
Revised March 04, 2025
Accepted March 13, 2025

Keywords
Cascaded Multilevel Inverters;
Asymmetric Inverters;
Selective Harmonic Elimination;
Bonobo Optimization Algorithm

ABSTRACT

Modern power electronics depend heavily on Multilevel Inverters (MLIs) to drive high-power systems operating in renewable energy systems electric vehicles along with industrial motor drives. MLIs create AC signals of high quality by joining multiple DC voltage sources which leads to minimal harmonic distortion outputs. The Cascaded H-Bridge MLI (CHB-MLI) stands out as a first choice among different topologies of MLI for photovoltaic (PV) applications because it includes modular features with fault tolerance capabilities and excellent multi-DC source integration. To achieve effective operation MLIs need optimized control strategies that reduce harmonics while maintaining highest performance. Using SHE-PWM technology provides an effective technique for harmonic frequency reduction which allows the improvement of waveform integrity. Technical restrictions make the solution of SHE-PWM nonlinear equations exceptionally challenging to implement. The resolution of complex non-linear equations requires implementation of GA combined with PSO and BO for optimal switching angle determination. The research investigates an 11-level asymmetric CHB-MLI using five solar panels where SHE-PWM switching angles are optimized through GA, PSO and BO applications. Simulation tests validate that the implemented algorithms succeed in minimizing Total Harmonic Distortion (THD) and removing fundamental harmonic disturbances. The evaluation demonstrates distinct capabilities of each optimization approach between accuracy rates and computational speed performance. These optimization methods yield practical advantages which boost the performance of multi-level inverters. The researchers who follow should study actual hardware deployments together with combined control approaches to enhance power electronic applications.

1. Introduction

The multilevel inverter stands as a vital power electronics device that produces highly powered AC waveforms through its stepped voltage design. These output waveforms are produced by MLIs by connecting multiple DC sources which both enhances efficiency and improves waveform quality. MLIs provide such advantages that make them standard devices in renewable energy systems along with electric vehicles, industrial motor drives and grid-connected power systems [1]-[4]. Multiple MLI topologies have evolved throughout time to boost inverter performance by resolving three primary issues regarding component numbers and commitment and harmonic elimination. The most popular multi-level inverter setups consist of three fundamental configurations which include Cascaded H-Bridge MLI (CHB-MLI), Diode-Clamped MLI (DC-MLI) and Capacitor-Clamped MLI (CC-MLI) [5]-[7]. The CHB-MLI incorporates H-bridge inverter units that operate with independent DC power supplies to achieve its functionality. The DC-MLI achieves stepwise voltage distribution through specific diode clamping and the CC-MLI enables stepped voltage levels using capacitors for improved voltage balancing purposes [8]-[10].

The Compound Hybrid Multilevel Inverter emerges as the optimal choice for implementing photovoltaic systems because of its distinguished features. The modular structure makes it an appropriate choice because it enables simple growth expansion capabilities. This multilevel inverter type shows optimal fault management abilities and makes it possible to connect various independent DC power sources efficiently. Renewable energy applications benefit greatly from the CHB-MLI since it provides an effective design with no need for passive components such as diodes or capacitors while eliminating the need for DC-MLI or CC-MLI extra equipment [11]-[14]. Major among the advantages of using MLI modules is their power to decrease harmonic distortion that enhances AC output quality. An MLI's stepped output waveform helps power conversion become more efficient because it eliminates the requirement for complex filtering. The distribution of voltage levels across several switching devices through MLIs reduces the individual semiconductor components' voltage exposure. Lower-rated devices can be implemented in the system because of this design trait which increases reliability and efficiency [15]-[18].

To achieve optimal performance from MLI systems it is essential to handle their existing challenges effectively. Higher-level inverters face an important operational challenge because they demand more components than lower-level inverters. The addition of each new voltage level raises the total count of power switches as well as driver circuits and passive components which generates more complex systems that cost more to build. The achievement of optimal switching angles for harmonic minimization needs complex control methods that increase overall inverter system complexity. The problem of DC source matching emerges specifically during asymmetric setups because unbalanced voltage distribution reduces system performance. The classification of MLIs depends on their DC voltage source distribution because it creates symmetric or asymmetric configuration patterns. Each DC source in symmetric MLIs operates with the same voltage amount which results in both balanced voltage distribution and easier control implementation. The operation of asymmetric MLIs depends on using sources with variable levels of DC voltage [19]-[24]. The asymmetric design enables inverter efficiency improvements by letting it produce stronger output voltage levels from reduced switching components but without circuit modifications. Symmetric MLIs offer the main benefit of producing elevated voltage outputs through fewer required switching devices. Further advanced control systems are required to maintain stable operation and optimal performance standards because asymmetric MLIs do not distribute their voltage equally.

The performance of MLIs depends fundamentally on control strategies because these strategies determine the operating methods of switching devices when creating desired output waveforms. Modulation technique selection stands equally important to circuit design principles for MLI operation [25]-[28]. Control methods applied to MLI systems comprise three distinct groups which include low-frequency switching operations and high-frequency switching operations and hybrid switching operations. The reduced number of switching transitions in low-frequency switching methods assists both high efficiency and reduced switching loss performance. The superiority of waveform quality

Vol. 5, No. 2, 2025, pp. 902-916

that high-frequency switching provides comes with higher switching losses because of its numerous switching events. Hybrid switching combines essential components from both low- and high-frequency techniques to reach an excellent balance between efficiency and performance standards [29]-[34].

The Selective Harmonic Elimination Pulse Width Modulation (SHE-PWM) represents an extensively studied modulation technique for Multi-Level Inverters (MLIs). The low-frequency switching technique SHE-PWM enables users to remove selected harmonic components that appear in the output waveform. The required optimal switching angles become known through solving the nonlinear transcendental equations [35]-[38]. An extensive amount of research exists about the SHE-PWM method because it provides superior waveform quality alongside lower switching frequencies to boost inverter efficiency. SHE-PWM presents a main obstacle due to its difficult nonlinear equation resolution requirements. The equations present solutions with multiple possibilities or without any solution that can be reached. The determination of precise optimal switching angles remains challenging for traditional methods because they need advanced optimization algorithms [39]-[43].

The research tackles SHE equation problems for an 11-level asymmetric CHB-MLI which operates with five solar panels. The main goal involves finding suitable switching angles for SHE-PWM with the help of advanced optimization techniques. This research implemented three distinct optimization algorithms which included Genetic Algorithm (GA) and Particle Swarm Optimization (PSO) with Bayesian Optimization (BO) as the last algorithm [4]-[8]. This bio-inspired optimization approach used within the Genetic Algorithm functions as a method to find excellent solutions through natural selection processes [44]-[48]. The effective solution of complex nonlinear problems within power electronics makes this method popular for diverse applications. PSO operates as an algorithm that draws inspiration from nature to study the movements of particles throughout their search space. PSO demonstrates both quick convergence speed and efficient computations that make it suitable for solving SHE equations. The probabilistic model-based Bayesian Optimization technique operates through efficient space exploration to find excellent solutions while consuming low computational resources [49]-[53]. The power electronics sector appreciates BO because of its strong nonlinearity restriction capabilities.

Simulation analysis was executed by using the optimal switching angles to assess the performance of these optimization methods. A thorough evaluation of the inverter output voltage profile along with harmonic content took place during various optimization condition tests. The evaluation of each optimization algorithm focused on Total Harmonic Distortion (THD) alongside specialized harmonic removal effectiveness for the 5th, 7th, 11th along with 13th harmonics and computational efficiency metrics. All optimization algorithms performed effectively to decrease harmonic distortion and enhance the quality of waveforms. The research evaluation showed unique advantages for each optimization method within its analysis. The SHE equation resolution by GA together with PSO demonstrated reliability yet BO achieved faster and lower-cost optimization solutions. this research establishes the advantageous performance of GA, PSO and BO algorithms when applied to finding SHE-PWM switching angle solutions in asymmetric 11-level CHB-MLI inverters. The implementation of these optimization methods results in improved inverter performance because they decrease THD levels and enhance power quality metrics. The experimental results showcase the practical value of advanced optimization techniques which find their most beneficial use in renewable energy systems coupled with high-power industrial drives. Future research will aim at three things: implementing optimized modulation methods directly on hardware systems and evaluating how different modulation methods work together for extra performance improvement.

2. Asymmetric Cascaded H-Bridge Inverter

Asymmetric cascaded H-bridge inverters are a subclass of cascaded H-bridge inverters. This type of inverter has a structure where each H-bridge rectifier has different DC sources. It is typically achieved by combining multiple DC sources with different voltage levels, which allows for higher voltage levels at the inverter's output. Asymmetric cascaded H-bridge inverters are used mainly in applications such as renewable energy systems. These inverters can integrate energy obtained from PV panels with different voltage levels into grid-connected AC systems. These inverters generally offer advantages such as high efficiency, low harmonic distortion, and wide operating range. However, the design and control processes should be carefully addressed to ensure the balanced utilization of different DC sources.

Fig. 1 presents the circuit design of the 11-level three-phase asymmetric CHB-MLI, while Fig. 2 presents the waveform of the single-phase output voltage. Output voltage level can be expressed as L=2x(VPV1+VPV2+VPV3) +1. Where VPV1 = Vdc, VPV2 = 2Vdc and VPV3= 2Vdc. Based on the switching angles for level 11, Table 1 presents the current status of the H-bridge module. The state '0' indicates that the module is not active, while the state '1' indicates that it is active. The modulation index, M, can be defined as the ratio of the output voltage to the total voltage (M=Vout/Vtotal). Vout is the maximum output voltage, and Vtotal is the total value of the input voltage sources (Vtotal=5Vdc).

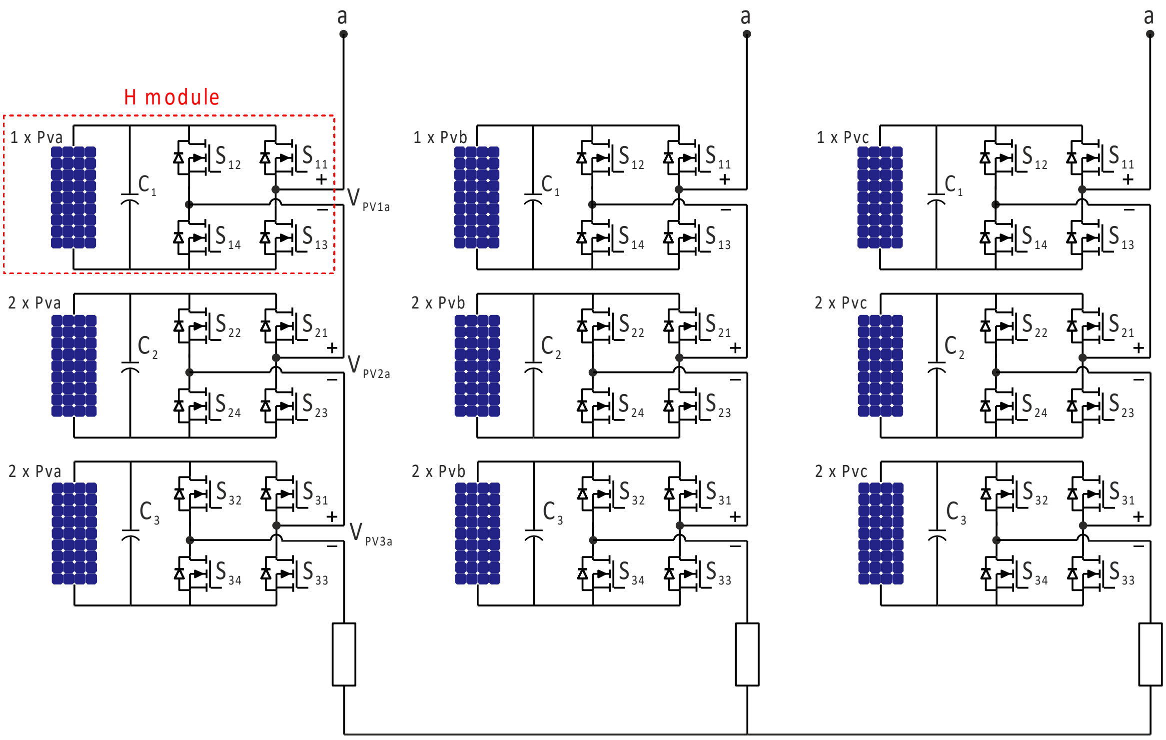

Fig. 1. Circuit of three-phase 11-level asymmetric CHB-MLI

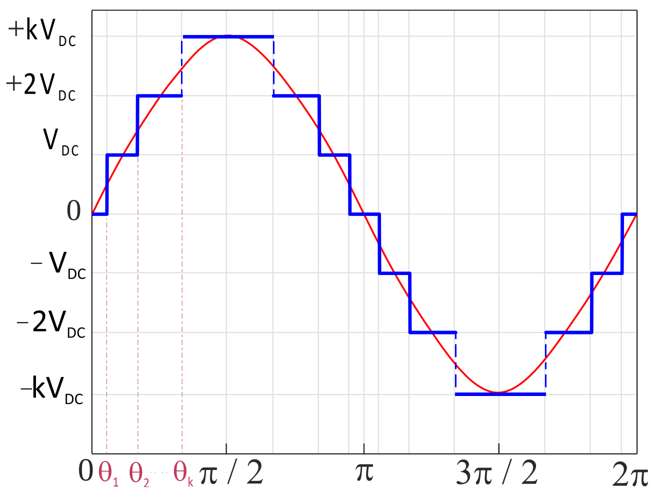

Fig. 2. Circuit of three-phase 11-level asymmetric CHB-MLI Output voltage waveform for single phase

3. Selective Harmonic Elimination

Selective Harmonic Elimination (SHE) is a control technique used in power electronics to eliminate specific harmonics from the output voltage waveform of inverters. The primary objective of SHE is to achieve a desired voltage waveform with reduced harmonic distortion by selectively eliminating specific harmonics while maintaining fundamental frequency components. This technique involves solving a set of nonlinear equations to determine the switching angles of the inverter, which allows for precise control over the harmonic content of the output voltage. By strategically selecting the switching angles, SHE enables the generation of high-quality output waveforms tailored to specific application requirements, such as grid-tie inverters for renewable energy systems [8]-[11].

Table 1. Module states in a quadrature

Module	The Switching Angles				
	θ_1	**θ_2**	**θ_3**	**θ_4**	**θ_5**
H_1	1	0	1	0	1
H_2	0	1	1	1	1
H_3	0	0	0	1	1

Equation (1) defines the nonlinear harmonic equations needed to determine the best switching angles in a 11-level CHB-MLI [13]-[16]. It expresses the output voltage, including all the harmonic components. The equation (1) allows us to determine the Vfund for the fundamental harmonic when n=1, and for the low order harmonics (n=5,7, 11, …) that we want to remove in three phase system.

$$\begin{aligned} V_{n^{th}} &= (V_{PV1})\,cos(n\theta_1) + (V_{PV2})\,cos(n\theta_2) + (V_{PV1} + V_{PV2})\,cos(n\theta_3) \\ &+ (V_{PV2} + V_{PV3})\,cos(n\theta_4) + (V_{PV1} + V_{PV2} + V_{PV3})\,cos(n\theta_5) \end{aligned} \tag{1}$$

The equations are solved in such a way that the value of Vfund is equal to the fundamental voltage value that is required, and that low-order harmonics, such as V5, V7, ...V13, are likewise determined to be zero. The THD value in three-phase systems may be determined using the equation (2). The highest limit for total harmonic distortion (THD) is infinite. The THDe value may be determined using the same procedure, which involves calculation up to the 13th harmonic. equation (3) calculates THD in three-phase systems. THD's highest harmonic limit is infinite. THDe may be calculated using the same procedure up to the 13th harmonic. The fitness function for Selective Harmonic Elimination Pulse Width Modulation (SHEPWM) in a 11-level inverter may be expressed as follows.

$$THD = \frac{\sqrt{V_5^2 + V_7^2 + V_{11}^2 \cdots}}{|V_1|} \tag{2}$$

$$\begin{gathered} f = \min_{\theta_i}\left\{\left|V_{fund} - V_{ref}\right| + \left(\left|V_{5^{rd}}\right|^2 + \ldots + \left|V_{13^{th}}\right|^2\right)\right\} = 0, \\ 0 \le \theta_1 < \theta_2 < \ldots < \theta_7 \le \frac{\pi}{2} \end{gathered} \tag{3}$$

4. Bonobo Optimization Algorithm

This article offers a concise introduction to the Bonobo Optimizer (BO) algorithm, a recently developed heuristic optimization technique. This algorithm is inspired by the social behaviors and mating techniques of bonobos [11]-[15] in its construction. Bonobos, similar to other primates, use a fission-fusion group strategy, wherein they split into smaller groups of different sizes (fusion) and autonomously explore their territory. Subsequently, they reintegrate (merge) with the rest of society to participate in customary activities, including engaging in sexual relations, competing with rivals, and so on. Bonobos use four separate reproductive strategies: consort ship mating, extra-group mating, restricted mating, and promiscuous mating, in addition to the aforementioned ones. The fundamental workings of these approaches exhibit a significant amount of diversity. The mathematical representation of the BO algorithm is as follows. The alpha bonobo, also known as the αbonobo, is referred to as the highest-ranking bonobo based on the objective value in this method.

Beginning with positive and negative phases, the BO algorithm considers two stages. Positive phase circumstances include abundant of food and shelter, great mating success, etc. Unlike the positive phase, the negative phase is the opposite. Each cycle increases positive phase count (ppc) and negative phase count (npc) by one and goes through a positive or negative phase. If one parameter is raised, the other is initialized to 0 [12].

The fusion social method helps bonobos pick mates. Equation (4) with the population size (N) may calculate the maximum temporary subgroup size (tsgsmax). For temporary sub-group size factor tsgsfactor, the maximum value of tsgsmax is between 2 and (tsgsfactor × N) [12].

$$tsgs\left(2,\left(tsg_{s_{\text{factor}}} \times N\right)\right)_{max} \tag{4}$$

We randomly choose a temporary subgroup size between 2 and tsgsmax. After then, the p th-bonobo gets mated since it has the greatest fitness in that subgroup. The positive phase favors restricted and promiscuous mating, whereas the negative phase favors consortship and extra-group mating. The BO algorithm calls this likelihood phase-probability (pp). The initial pp value is 0.5. This value is adjusted after each iteration depending on the phase and number of phases. During positive phases, it ranges (0.5, 1.0); during negative phases, (0, 0.5). The main positive phase equation (5) [12].

$$\begin{aligned} \text{new\_bonobo}_j = {} & \text{bonobo}_j^i + r_1 \times scab \times \left(\alpha_{\text{bonobo}}^j - \text{bonobo}_j^i\right) \\ & +(1-r_1) \times scsb \times \text{ flag } \times \left(\text{bonobo}_j^i - \text{bonobo}_j^p\right) \end{aligned} \tag{5}$$

Alpha bonobo and offspring have j-variables bonobo and new bonoboj. The optimization problem has d variables, and j ranges from 1 to d. Sharing parameters are scab and scsb. Flag is given 1 or -1 depending on the circumstance. equations (6)-(11) create the new bonobo during extra-group mating in a negative phase [12].

$$\beta_1 = e^{\left(r_1^2 + r_1 - 2/r_1\right)} \tag{6}$$

$$\beta_2 = e^{\left(-r_1^2 + 2 \times r_1 - 2/r_1\right)} \tag{7}$$

$$\text{new\_bonobo}_j = \text{bonobo}_j^i + \beta_1 \times \left(\text{Var\_max}_j - \text{bonobo}_j^i\right) \tag{8}$$

$$\text{new\_bonobo}_j = \text{bonobo}_j^i - \beta_2 \times \left(\text{bonobo}_j^i - \text{Var\_}\underset{j}{min}\right) \tag{9}$$

$$\text{new\_bonobo}_j = \text{bonobo}_j^i - \beta_1 \times \left(\text{bonobo}_j^i - \text{Var\_}\underset{j}{min}\right) \tag{10}$$

$$\text{new\_bonobo}_j = \text{bonobo}_j^i + \beta_2 \times \left(\text{Var\_}\underset{j}{max} - \text{bonobo}_j^i\right) \tag{11}$$

Fig. 3, titled "Fission-fusion social groups of bonobos," illustrates the dynamic social structure of bonobos. This system is characterized by individuals splitting into smaller subgroups (fission) and reuniting into larger groups (fusion) over time. The main group typically consists of individuals sharing a specific territory, but they may divide into smaller units based on resource availability or social bonds. These subgroups later merge again for social interactions or other needs. This system demonstrates the social flexibility and complex relationships within bonobo communities. Fig. 4 illustrates the movement directions of different bonobos in two areas, PP and NP, highlighting the paths with higher probabilities. This provides insights into how bonobos navigate their environment, likely influenced by factors such as resource distribution, social interactions, and environmental conditions. Understanding these patterns aids in optimizing strategies for bonobo conservation and habitat management by focusing on critical movement corridors and high-use areas.

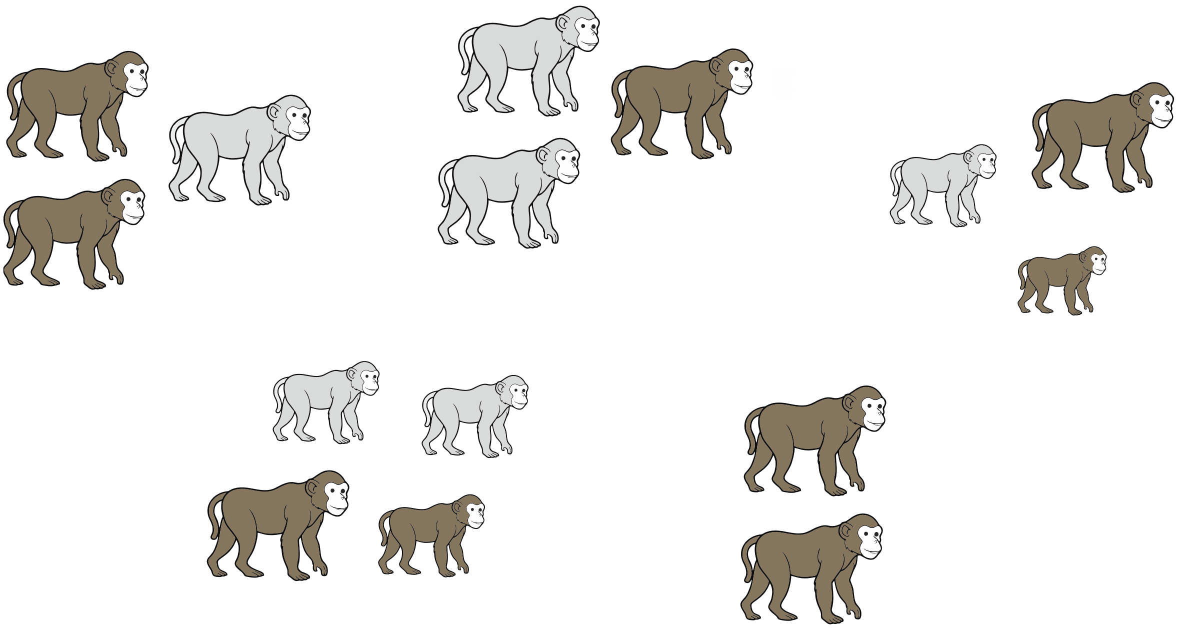

Fig. 3. Fission-fusion social groups of bonobos [12]

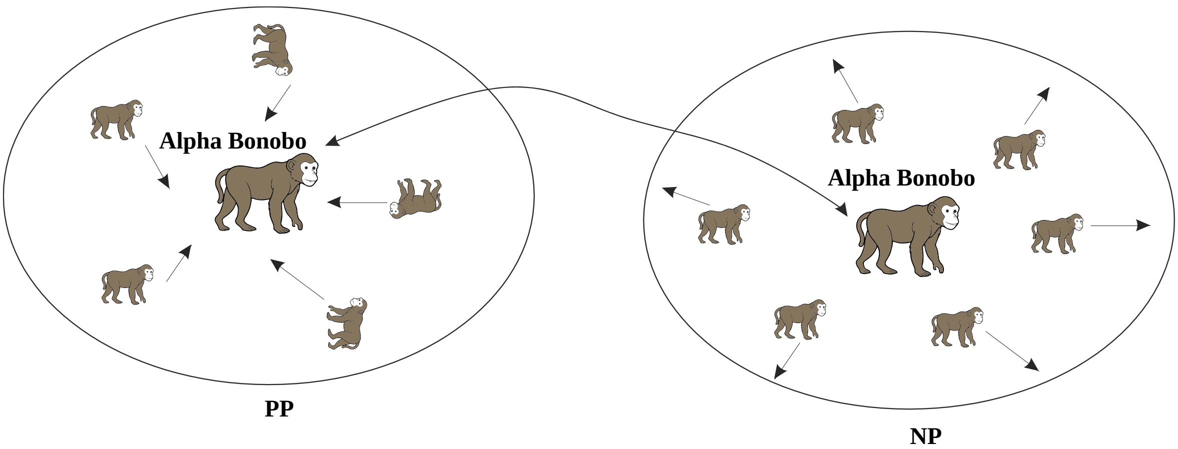

Fig. 4. Directions of movements of different bonobos in PP and NP with the higher probabilities [12]

A flowchart explaining the proposed BO is shown in Fig. 5. It is also important to note that the suggested technique generates all of the random integers that are utilized in the range of (0.0, 1.0). The two intermediate variables are and, and the jth variable's lower and upper limits are Var_maxj and Var_minj. R1 is random and between 0 and 1. See [12] for equation use criteria. Each cycle finishes with search feedback, which is utilized to alter controlling parameters and concentrate on promising variable space areas.

5. Simulation Results

To calculate the optimal switching angles for SHE-PWM, GA, PSO, and BO algorithms were implemented using MATLAB. The switching angles obtained through GA are presented in Table 2, those obtained through PSO in Table 3, and finally, the angles calculated using BO in Table 4. For each modulation level, the determined switching angles were applied to the inverter, and the resulting output voltage and harmonic analysis are displayed separately in each table. All algorithms were able to find solutions within the modulation index range of 0.1 to 1.0. However, the weakest solutions were obtained with the GA, while the strongest solutions were achieved using the BO algorithm. mAlthough GA controlled the fundamental voltage well, it obtained worse results than the other algorithms for all modulation index values. The GA algorithm effectively controlled the fundamental voltage error and suppressed selected harmonics between modulation indices of 0.5 and 1.0. The PSO algorithm controlled the fundamental voltage error more effectively than the GA algorithm and suppressed selected harmonics between modulation indices of 0.7 and 1.0. The BO algorithm effectively controlled the fundamental voltage error and suppressed selected harmonics between modulation indices of 0.5 and 1.0.

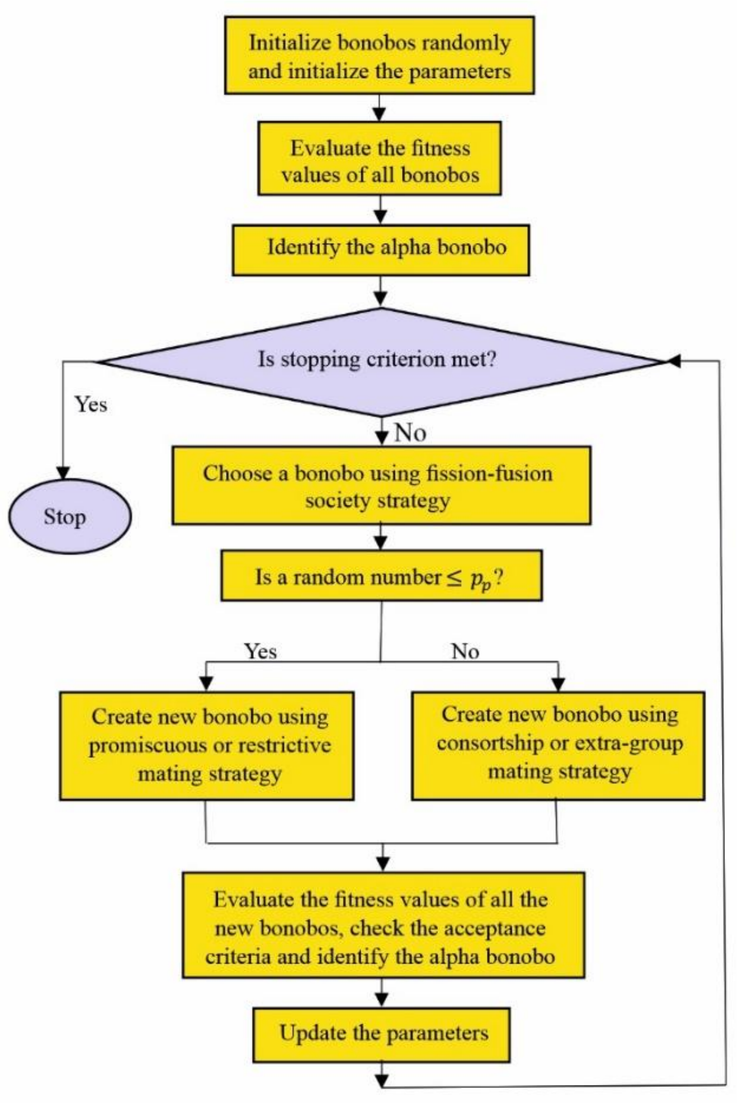

Fig. 5. Flowchart of the proposed algorithm BO [12]

The convergence curve for a unit modulation index is presented in Fig. 6. As observed, the BO algorithm exhibits the most effective convergence behavior, achieving superior optimization performance compared to the other methods. In contrast, the GA algorithm demonstrates the least efficient convergence characteristics. The PSO algorithm outperforms GA but falls short of the convergence efficiency achieved by the BO algorithm. All algorithms achieved their optimal Total Harmonic Distortion (THD) performance at a modulation index of 1.0. The corresponding results are illustrated in Fig. 7 for the GA algorithm, Fig. 8 for the PSO algorithm, and Fig. 9 for the BO algorithm, respectively.

Table 2. Results Of GA Based Mli

M	SWITCHING ANGLES (radian)					LOAD VOLTAGE			HARMONIC VALUES (%)					
	θ_1	θ_2	θ_3	θ_4	θ_5	Vref (max)	V1p (max)	Error (%)	THD	THDe	5th	7th	11th	13th
0.1	1.27600	1.52400	1.52400	1.56800	1.56800	25	24.69	1.24%	116.31	98.75	76.41	57.46	21.94	11.32
0.2	0.71000	1.56400	1.56400	1.56400	1.56400	50	49.84	0.32%	27.54	21.12	19.92	1.24	3.03	6.19
0.3	0.92400	0.99300	1.56100	1.56100	1.56100	75	74.78	0.29%	28.74	25.85	5.25	18.96	8.77	14.29
0.4	0.73600	0.73600	1.53600	1.54400	1.54400	100	99.7	0.30%	29.17	18.87	16.27	2.06	8.38	4.11
0.5	0.71300	0.90500	1.15500	1.42700	1.52900	125	124.5	0.40%	13.57	9.09	6.56	0.63	6.05	1.59
0.6	0.79900	0.79900	0.95900	1.31100	1.43900	150	149.5	0.33%	15.32	13.92	2.88	4.14	12.82	1.98
0.7	0.41100	0.72700	0.89500	1.14300	1.52700	175	174.3	0.40%	9.43	4.48	3.82	0.21	2.33	0.17
0.8	0.65200	0.78000	0.79600	1.08400	1.08400	200	199.1	0.45%	14.99	11.95	6.94	8.27	2.27	4.58
0.9	0.28500	0.44500	0.63900	1.08500	1.15100	225	224.4	0.27%	9.76	8.18	0.31	6.46	4.41	2.40
1.0	0.13000	0.32200	0.64200	0.76200	1.09000	250	249.0	0.40%	6.65	4.86	1.79	2.11	0.60	3.95

Table 3. Results Of PSO Based Mli

M	SWITCHING ANGLES (radian)					LOAD VOLTAGE			HARMONIC VALUES (%)					
	θ_1	θ_2	θ_3	θ_4	θ_5	Vref (max)	V1p (max)	Error (%)	THD	THDe	5th	7th	11th	13th
0.1	1.16723	1.57080	1.57080	1.57080	1.57080	25	24.91	0.36%	59.35	55.17	46.09	11.48	22.31	17.01
0.2	0.66746	1.57080	1.57080	1.57080	1.57080	50	49.87	0.26%	29.03	26.67	25.03	0.78	5.72	7.18
0.3	0.77478	1.13258	1.53538	1.56701	1.57080	75	74.73	0.36%	19.81	8.17	4.56	3.71	0.39	5.67
0.4	0.32068	0.89979	1.57080	1.57080	1.57080	100	99.68	0.32%	11.32	11.52	3.15	3.42	10.53	0.63
0.5	0.12742	0.65141	1.39441	1.56990	1.57079	125	124.6	0.32%	10.28	6.99	6.00	3.50	0.68	0.40
0.6	0.21374	0.63763	1.04395	1.53447	1.53447	150	149.5	0.33%	10.23	3.19	2.82	1.01	1.06	0.32
0.7	0.06389	0.66935	0.71473	1.38919	1.53996	175	174.3	0.40%	7.60	0.12	0.05	0.02	0.10	0.05
0.8	0.16272	0.44239	0.74020	1.07009	1.53810	200	199.2	0.40%	6.71	0.04	0.01	0.02	0.00	0.02
0.9	0.28403	0.45293	0.78201	1.06684	1.06694	225	224.1	0.40%	7.12	0.47	0.25	0.15	0.14	0.33
1.0	0.13717	0.33811	0.51753	0.83217	1.10327	250	249.0	0.40%	5.03	0.04	0.01	0.01	0.03	0.02

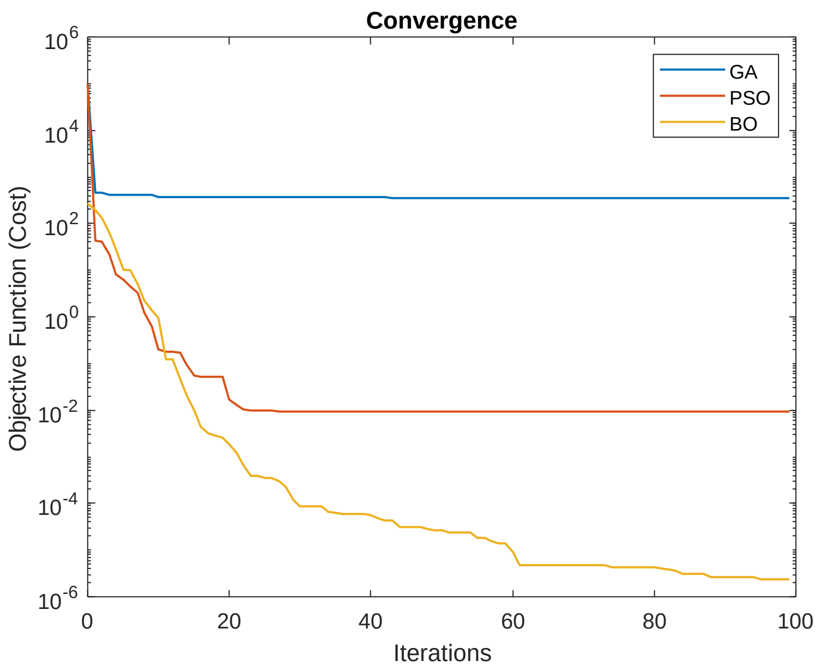

Fig. 6. Convergence curve of GA, PSO and BO for unit modulation index

The output voltage waveform for a unit modulation index calculated using GA is depicted in Fig. 7 (a). The fundamental voltage was achieved with a maximum value of 249V, resulting in an error of 0.40%. The corresponding THD and THDe values were computed as 6.65% and 4.86%, respectively, as shown graphically in Fig. 7 (b) and (c). For the unit modulation index, the output voltage waveform calculated with PSO is shown in Fig. 8 (a). The fundamental voltage reached a maximum of 249V with a 0.40% error. The THD and THDe values were determined to be 5.03% and 0.04%, respectively, and are displayed in graphical form in Fig. 8 (b) and (c).

Table 4. Results Of BO Based Mli

M	SWITCHING ANGLES (radian)					LOAD VOLTAGE			HARMONIC VALUES (%)					
	θ_1	θ_2	θ_3	θ_4	θ_5	Vref (max)	V1p (max)	Error (%)	THD	THDe	5th	7th	11th	13th
0.1	1.16723	1.5708	1.5708	1.5708	1.5708	25	24.91	0.36%	59.34	55.16	46.09	11.47	22.31	17.00
0.2	0.75459	1.51392	1.5708	1.5708	1.5708	50	49.84	0.32%	27.67	18.29	13.45	2.74	11.85	2.41
0.3	0.75368	1.10524	1.5708	1.5708	1.5708	75	74.84	0.21%	17.37	11.72	1.40	7.92	3.87	7.59
0.4	0.68834	0.98613	1.32165	1.5708	1.5708	100	99.67	0.33%	12.81	3.14	2.68	0.55	1.55	0.07
0.5	0.64076	0.86624	1.14344	1.47094	1.5708	125	124.6	0.32%	**9.04**	**1.06**	**0.50**	**0.31**	**0.78**	**0.41**
0.6	0.61666	0.81819	1.0206	1.26371	1.53045	150	150	0.00%	**6.89**	**0.06**	**0.02**	**0.02**	**0.03**	**0.03**
0.7	0.59585	0.78095	0.94101	1.13994	1.35455	175	175	0.00%	**5.55**	**0.07**	**0.03**	**0.03**	**0.01**	**0.02**
0.8	0.1603	0.43475	0.73238	1.06608	1.53871	200	200	0.00%	**6.46**	**0.05**	**0.01**	**0.01**	**0.03**	**0.01**
0.9	0.12856	0.47373	0.70783	0.91053	1.27352	225	225	0.00%	**6.12**	**0.03**	**0.02**	**0.00**	**0.01**	**0.01**
1.0	0.13223	0.33598	0.5083	0.82256	1.10019	250	250	0.00%	**4.84**	**0.04**	**0.01**	**0.01**	**0.00**	**0.03**

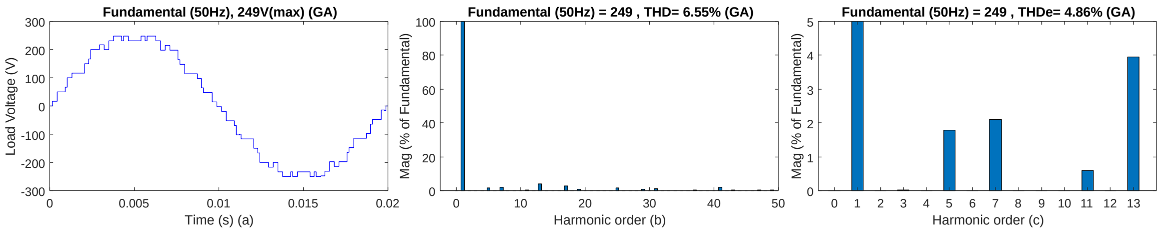

Fig. 7. Performance of the GA Algorithm at M=1.0: a) Output Voltage Waveform, b THD, c) THDe

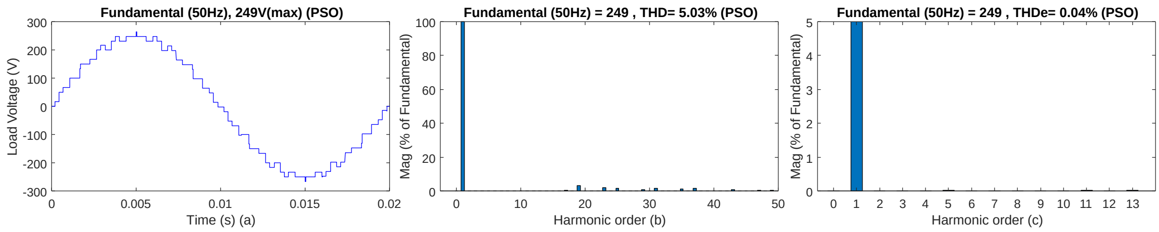

Fig. 8. Performance of the PSO Algorithm at M=1.0: a) Output Voltage Waveform, b THD, c) THDe

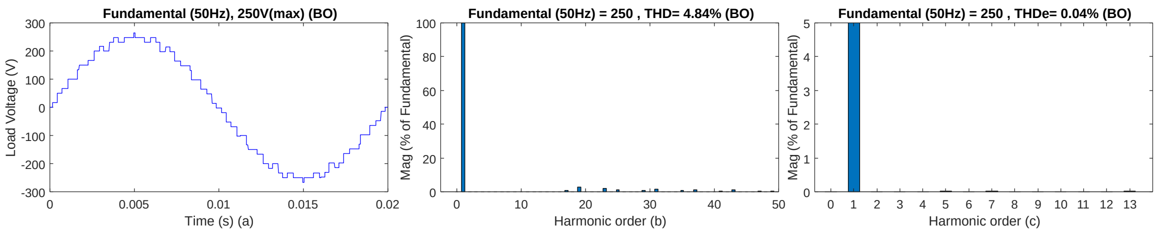

Fig. 9. Performance of the BO Algorithm at M=1.0: a) Output Voltage Waveform, b THD, c) THDe

The output voltage waveform for a unit modulation index, calculated using BO, is presented in Fig. 9 (a). The fundamental voltage was attained with a maximum value of 250V, with no error (0.0%). The THD and THDe values were found to be 4.84% and 0.04%, respectively, and are illustrated in Fig. 9 (b) and (c).

6. Conclusion

When comparing the performance of the three algorithms (GA, PSO, and BO) in terms of THD, 5th harmonic, 7th harmonic, 11th harmonic, and 13th harmonic, it is observed that the BO algorithm provides the best overall performance. In terms of THD (Total Harmonic Distortion), the BO algorithm achieves the lowest values compared to the other two algorithms, providing the cleanest output. The THD values for BO range from a maximum of 59.34% at 25V to a minimum of 4.84% at 250V, while PSO shows a maximum of 59.35% and a minimum of 5.03%, and GA shows a maximum of 116.31% and a minimum of 6.65%. This indicates that the BO algorithm provides the most efficient performance with lower overall distortion levels.

For the 5th harmonic, GA shows higher values initially (76.41% at 25V), but these values decrease significantly as the load voltage increases, with the lowest value being 1.79% at 250V. PSO starts with lower values and shows a maximum of 46.09% at 25V and a minimum of 0.01% at 250V. Similarly, BO's 5th harmonic values also remain low, with the highest value being 46.09% at 25V and the lowest 0.01% at 250V. For the 7th harmonic, GA exhibits high values, especially at lower voltages (57.46% at 25V), but these values decrease as voltage increases, reaching 2.11% at 250V. PSO performs better than GA in terms of stability, with the highest 7th harmonic at 22.31% (25V) and the lowest at 0.01% (250V). BO shows similarly low levels for the 7th harmonic, with the highest value at 7.92% (75V) and the lowest at 0.03% (250V).

Looking at the 11th harmonic, GA shows higher values at lower voltages (21.94% at 25V), but these values decrease with higher voltages, reaching 0.60% at 250V. In PSO, 11th harmonic values are also lower, improving with voltage increase. The maximum value is 19.92% (50V), and the minimum value is 0.03% (250V). BO performs even better, with the highest 11th harmonic value at 7.59% (75V) and the lowest at 0.00% (250V). Finally, for the 13th harmonic, GA shows higher values initially (11.32% at 25V), but these decrease as voltage increases, with the lowest value at 3.95% at 250V. In PSO, the 13th harmonic shows a maximum of 17.01% at 25V, and the minimum value is 0.02% at 250V. BO shows the lowest values overall for the 13th harmonic, with a maximum of 17.00% at 25V and a minimum of 0.03% at 250V.

In conclusion, the BO algorithm provides the best performance overall by achieving the lowest THD and harmonic values, offering the cleanest and most stable results. PSO performs better than GA, showing lower harmonic levels, but still falls behind BO. GA starts with higher distortion levels, which decrease as the load voltage increases, but it remains less efficient compared to BO and PSO. Therefore, the BO algorithm stands out by offering the least distortion and the most stable performance with minimal harmonic contributions. Recent advancements in Bonobo Optimization (BO) have proven highly effective in optimizing switching angles, particularly in mitigating selected harmonics within 11-level Cascaded H-Bridge Multilevel Inverter (CHB-MLI) systems employing asymmetric DC sources such as photovoltaic (PV) panels. The theoretical analysis was corroborated through simulation conducted on a three-phase 11-level CHB-MLI, thereby validating the proposed approach.

Author Contribution: All authors contributed equally to the main contributor to this paper. All authors read and approved the final paper.

Funding: This research received no external funding.

Conflicts of Interest: The authors declare no conflict of interest.

References

[1] M. Pamujula, A. Ohja, R. D. Kulkarni and P. Swarnkar, "Cascaded 'H' Bridge based Multilevel Inverter Topologies: A Review," *2020 International Conference for Emerging Technology (INCET)*, pp. 1-7, 2020, https://doi.org/10.1109/incet49848.2020.9154031.

[2] R. Pawar, S. P. Gawande, S. G. Kadwane, M. A. Waghmare, R. N. Nagpure, "Five-level diode clamped multilevel inverter (DCMLI) based electric spring for smart grid applications," *Energy Procedia*, vol. 117, pp. 862-869, 2017, https://doi.org/10.1016/j.egypro.2017.05.204.

[3] R. Castillo, B. Diong, P. Biggers, "Single-phase hybrid cascaded H-bridge and diode-clamped multilevel inverter with capacitor voltage balancing," *IET Power Electronics*, vol. 11, no. 4, pp. 700-707, 2018, https://doi.org/10.1049/iet-pel.2017.0009.

[4] V. Sridhar, S. Umashankar, “A comprehensive review on CHB MLI based PV inverter and feasibility study of CHB MLI based PV-STATCOM,” *Renewable and Sustainable Energy Reviews*, vol. 78, pp. 138-156, 2017, https://doi.org/10.1016/j.rser.2017.04.111.

[5] P. S. Subudhi, A. R. Kumar, S. Krithiga, T. Deepa, S. Padmanaban and D. P. Kothari, "Simulation Analysis of Selective Harmonics Elimination scheme for a Symmetric CHB-Multilevel inverter," *2019 Innovations in Power and Advanced Computing Technologies (i-PACT)*, pp. 1-4, 2019, https://doi.org/10.1109/i-pact44901.2019.8960242.

[6] M. Saeedian, J. Adabi, S. M. Hosseini, “Cascaded multilevel inverter based on symmetric–asymmetric DC sources with reduced number of components,” *IET Power Electronics*, vol. 10, no. 12, pp. 1468-1478, 2017, https://doi.org/10.1049/iet-pel.2017.0039.

[7] S. Chatterjee, A. Das, “A review on technological aspects of different PWM techniques and its comparison based on different performance parameters,” *International Journal of Circuit Theory and Applications*, vol. 51, no. 5, pp. 2446-2498, 2023, https://doi.org/10.1002/cta.3513.

[8] Y. Bektaş and H. Karaca, "Red Deer Algorithm Based Harmonic Mitigation for Asymmetric Cascaded Multilevel Inverters," *2022 57th International Scientific Conference on Information, Communication and Energy Systems and Technologies (ICEST)*, pp. 1-4, 2022, https://doi.org/10.1109/icest55168.2022.9828611.

[9] Y. Bektaş, H. Karaca, T. A. Taha, H. I. Zaynal, “Red deer algorithm-based selective harmonic elimination technique for multilevel inverters,” *Bulletin of Electrical Engineering and Informatics*, vol. 12, no. 5, pp. 2643-2650, 2023, https://doi.org/10.11591/eei.v12i5.5160.

[10] Y. Bektaş, “Real-time control of Selective Harmonic Elimination in a Reduced Switch Multilevel Inverter with unequal DC sources,” *Ain Shams Engineering Journal*, vol. 15, no. 6, p. 102719, 2024, https://doi.org/10.1016/j.asej.2024.102719.

[11] A. K. Das and D. K. Pratihar, "A New Bonobo optimizer (BO) for Real-Parameter optimization," *2019 IEEE Region 10 Symposium (TENSYMP)*, pp. 108-113, 2019, https://doi.org/10.1109/tensymp46218.2019.8971108.

[12] A. K. Das, D. K. Pratihar, “Bonobo optimizer (BO): an intelligent heuristic with self-adjusting parameters over continuous spaces and its applications to engineering problems,” *Applied Intelligence*, vol. 52, no. 3, pp. 2942-2974, 2022, https://doi.org/10.1007/s10489-021-02444-w.

[13] H. Juma'a, T. Atyia, “Design and Implementation of multi-level inverter for PV system with various DC Sources,” *NTU Journal of Renewable Energy*, vol. 5, no. 1, pp. 24-33, 2023, https://doi.org/10.56286/ntujre.v5i1.554.

[14] Z. Ali, Z. M. Abdullah, B. A. Naser, R. W. Daoud, A. H. Ahmed, “Design of a Single-Phase Inverter for Solar Energy Conversion System,” *NTU Journal of Renewable Energy*, vol. 1, no. 1, pp. 38-42, 2021, https://doi.org/10.56286/ntujre.v1i1.13.

[15] E. H. I. Albajari, S. R. Aslan, “Exploring the Synergy of Integration: Assessing the Performance of Hydraulic Storage and Solar Power Integration in Kirkuk city,” *NTU Journal of Renewable Energy*, vol. 5, no. 1, pp. 1-7, 2023, https://doi.org/10.56286/ntujre.v5i1.525.

[16] P. Gagneux, C. Boesch, D. S. Woodruff, “Female reproductive strategies, paternity and community structure in wild West African chimpanzees,” *Animal Behaviour*, vol. 57, no. 1, pp. 19-32, 1999, https://doi.org/10.1006/anbe.1998.0972.

[17] B. Sharma, S. Manna, V. Saxena, P. K. Raghuvanshi, M. H. Alsharif, M. K. Kim, “A comprehensive review of multi-level inverters, modulation, and control for grid-interfaced solar PV systems,” *Scientific reports*, vol. 15, no. 1, p. 661, 2025, https://doi.org/10.1038/s41598-024-84296-1.

[18] A. M. Abdel-Hamed, A. M. Nasser, H. Shatla, A. Refky, “An improved SPWM control approach with aid of ant lion optimization for minimizing the THD in multilevel inverters,” *Scientific Reports*, vol. 15, no. 1, p. 1990, 2025, https://doi.org/10.1038/s41598-024-84678-5.

[19] M. S. Hossain, N. A. M. Said, M. A. Hasan, W. A. Halim, W. N. W. A. Munim, A. Jidin, “Performance evaluation of a nearest level control-based TCHB multilevel inverter for PMSM motors in electric vehicle

systems," *Results in Engineering*, vol. 25, p. 103949, 2025, https://doi.org/10.1016/j.rineng.2025.103949.

[20] A. Singh, V. Jately, P. Kala, Y. Yang, "Enhancing power quality in electric vehicles and battery energy storage systems using multilevel inverter topologies–A review," *Journal of Energy Storage*, vol. 110, p. 115274, 2025, https://doi.org/10.1016/j.est.2024.115274.

[21] H. Mansourizadeh, M. Hosseinpour, A. Seifi, M. Shahparasti, "A 13-level switched-capacitor-based multilevel inverter with reduced components and inrush current limitation," *Scientific Reports*, vol. 15, no. 1, p. 290, 2025, https://doi.org/10.1038/s41598-024-84148-y.

[22] C. H. Lin, S. A. Farooqui, H. D. Liu, A. Sarwar, M. Zaid, J. Ahmad, "Performance enhancement of a multilevel inverter in renewable energy systems using equilibrium optimizer," *Electric Power Systems Research*, vol. 243, p. 111538, 2025, https://doi.org/10.1016/j.epsr.2025.111538.

[23] M. H. Mondol, M. A. Rahman, S. P. Biswas, M. R. Islam, M. F. Kibria and K. M. Muttaqi, "A New Integrated Multilevel Inverter Topology for Renewable Energy Transformation," *IEEE Transactions on Industry Applications*, vol. 59, no. 3, pp. 3031-3043, 2023, https://doi.org/10.1109/tia.2023.3246461.

[24] P. Matt, L. Roslaniec, M. Gantner, "3-Level GaN Inverters for Highly Efficient Power Electronics in Electric Vehicles," *MTZ worldwide*, vol. 86, no. 2, pp. 40-43, 2025, https://doi.org/10.1007/s3831302420230.

[25] S. Gao, Z. Jiang, F. Pang, S. Zhao, "A Novel Modular Expandable Multilevel Converter," *International Journal of Circuit Theory and Applications*, 2025, https://doi.org/10.1002/cta.4429.

[26] K. Ramu *et al*., "Smart solar power Conversion: Leveraging Deep learning MPPT and hybrid cascaded h-bridge multilevel inverters for optimal efficiency," *Biomedical Signal Processing and Control*, vol. 105, p. 107582, 2025, https://doi.org/10.1016/j.bspc.2025.107582.

[27] S. Agrawal, S. K. Kuncham and M. Sahoo, "A Fault-Tolerant Common-Ground based Five-Level Inverter for Photovoltaic Applications," *IEEE Journal of Emerging and Selected Topics in Industrial Electronics*, pp. 1-8, 2024, https://doi.org/10.1109/jestie.2024.3503282.

[28] S. Q. Salih *et al*., "Enhanced Total Harmonic Distortion Optimization in Cascaded H-Bridge Multilevel Inverters Using the Dwarf Mongoose Optimization Algorithm," *Journal of Robotics and Control (JRC)*, vol. 5, no. 6, pp. 1862-1871, 2024, https://doi.org/10.18196/jrc.v5i6.23548.

[29] R. I. H. Hussein *et al*., "Enhanced transformer protection using fuzzy-logic-integrated differential relays: a comparative study with rule-based methods," *Journal of Robotics and Control (JRC)*, vol. 5, no. 5, pp. 1299-1310, 2024, https://doi.org/10.18196/jrc.v5i5.21937.

[30] T. A. Taha *et al*., "Enhancing Multilevel Inverter Performance: A Novel Dung Beetle Optimizer-based Selective Harmonic Elimination Approach," *Journal of Robotics and Control (JRC)*, vol. 5, no. 4, pp. 944-953, 2024, https://doi.org/10.18196/jrc.v5i4.21722.

[31] T. A. Taha, N. I. A. Wahab, M. K. Hassan, H. I. Zaynal, F. H. Taha, A. M. Hashim, "Real-Time Optimal Switching Angle Scheme for a Cascaded H-Bridge Inverter using Bonobo Optimizer," *Journal of Robotics and Control (JRC)*, vol. 5, no. 4, pp. 918-930, 2024, https://doi.org/10.18196/jrc.v5i4.21701.

[32] A. S. T. Hussain et al., "Unlocking solar potential: advancements in automated solar tracking systems for enhanced energy utilization," *Journal of Robotics and Control (JRC)*, vol. 5, no. 4, pp. 1018-1027, 2024, https://doi.org/10.18196/jrc.v5i4.19931.

[33] E. Bektaş *et al*., "Enhancing Harmonic Reduction in Multilevel Inverters using the Weevil Damage Optimization Algorithm," *Journal of Robotics and Control (JRC)*, vol. 5, no. 3, pp. 717-722, 2024, https://doi.org/10.18196/jrc.v5i3.21544.

[34] D. David, A. Alamoodi, "A bibliometric analysis of research on multiple criteria decision making with emphasis on Energy Sector between (2019-2023)," *Applied Data Science and Analysis*, pp. 143-149, 2023, https://doi.org/10.58496/adsa/2023/013.

[35] J. F. Ardashir, M. Hasannezhad, H. V. Ghadim, M. Sarhangzadeh, "Integration of energy storage systems with multilevel inverters for microgrids," *Distributed Energy Storage Systems for Digital Power Systems*, pp. 293-318, 2025, https://doi.org/10.1016/b978-0-443-22013-5.00012-5.

[36] S. M. Alqaraghuli, O. Karan, "Using deep learning technology based energy-saving for software defined wireless sensor networks (SDWSN) framework," *Babylonian Journal of Artificial Intelligence*, vol. 2024, pp. 34-45, 2024, https://doi.org/10.58496/bjai/2024/006.

[37] R. Sahoo, A. Tiwari, M. Roy, "Advanced self-balanced seven-level inverter topology based on symmetrical capacitors with voltage-boosting capability," *Electrical Engineering*, vol. 1-18, 2025, https://doi.org/10.1007/s00202-025-02951-w.

[38] N. Jin, J. Yang, J. Hou, M. Gao, D. Sun, "Research on Optimized Multi-Objective FCS-MPC Without Weighting Factors of NPC Three-Level Inverter," *International Journal of Circuit Theory and Applications*, 2025, https://doi.org/10.1002/cta.4449.

[39] Y. E. Ahmed, "Intelligent watering by using solar energy system," *Babylonian Journal of Internet of Things*, pp. 53-59, 2024, https://doi.org/10.58496/bjiot/2024/007.

[40] C. Ali *et al.*, "An Enhanced Active Disturbance Rejection Control Scheme for DC Voltage Regulation in Photovoltaic Grid-Connected Four-Leg Inverter Using a Sliding Mode Observer," *IEEE Access*, vol. 13, pp. 18623-18643, 2025, https://doi.org/10.1109/access.2025.3533015.

[41] P. K. Dutta, S. M. El-kenawy, G. Ali, K. Dhoska, "An Energy consumption monitoring and control system in buildings using internet of things," *Babylonian Journal of Internet of Things*, pp. 38-47, 2023, https://doi.org/10.58496/bjiot/2023/006.

[42] S. Khettab, A. Kheldoun, R. Bradai, "A novel Runge-Kutta-based model predictive controller for PUC7-based single-phase shunt active power filter," *Computers and Electrical Engineering*, vol. 123, p. 110051, 2025, https://doi.org/10.1016/j.compeleceng.2024.110051.

[43] M. N. Hamidi, D. Ishak, "Jordan Journal of Electrical Engineering," *Jordan Journal of Electrical Engineering*, vol. 11, no. 1, pp. 180-197, 2025, https://doi.org/10.5455/jjee.204-1725866221.

[44] S. Gao, Z. Jiang, F. Pang, S. Zhao, "A Novel Modular Expandable Multilevel Converter," *International Journal of Circuit Theory and Applications*, 2025, https://doi.org/10.1002/cta.4429.

[45] A. Fathollahi and B. Andresen, "Power Quality Analysis and Improvement of Power-to-X Plants Using Digital Twins: A Practical Application in Denmark," *IEEE Transactions on Energy Conversion*, pp. 1-12, 2025, https://doi.org/10.1109/tec.2025.3531113.

[46] S. H. Ahmed, "An analytical study on improving target tracking techniques in wireless sensor networks using deep learning and energy efficiency models," *Babylonian Journal of Networking*, pp. 100-104, 2023, https://doi.org/10.58496/bjn/2023/013.

[47] S. M. Baraa, H. Desa, K. S. Mohammed, T. A. Al-Malaisi, A. S. T. Hussain, H. S. Majdi, "Selective Harmonic Elimination in Reduced-Switch Multilevel Inverters for PV Systems Using the Sparrow Search Algorithm," *Journal of Robotics and Control (JRC)*, vol. 6, no. 1, pp. 385-395, 2025, https://journal.umy.ac.id/index.php/jrc/article/view/25108.

[48] V. T. Pardhi, R. Pottekkat, V. R. S., K. Gopakumar, L. Umanand and D. Zielinski, "A Single DC Source Multilevel Inverter for Drives With Increasing Linear Modulation Range and Fault Tolerant Capability," *IEEE Transactions on Industrial Electronics*, pp. 1-10, 2025, https://doi.org/10.1109/tie.2025.3532615.

[49] H. Rehman, M. Tariq, C. -H. Chang, A. Sarwar, S. Ahmad and a. Hwa-Dong Liu, "A Boat Type Fault Tolerant Multilevel Inverter Topology Resilient to Switch Fault," *IEEE Access*, vol. 13, pp. 31368-31384, 2025, https://doi.org/10.1109/access.2025.3541172.

[50] D. Krishnachaitanya, C. Annamalai, M. Al-Greer, S. S. Biswas, "A novel reliability estimation methodology towards the design and implementation of symmetric multilevel inverter for long run applications," *IET Power Electronics*, vol. 18, no. 1, p. e12843, 2025, https://doi.org/10.1049/pel2.12843.

[51] O. F. Ozcan, H. Kilic, O. F. Ozguven, "A unified robust hybrid optimized Takagi–Sugeno fuzzy control for hydrogen fuel cell-integrated microgrids," *International Journal of Hydrogen Energy*, 2025, https://doi.org/10.1016/j.ijhydene.2025.01.337.

[52] E. Zaidi, K. Marouani, H. Bouadi, A. E. Kassel, L. Bentouhami and E. Merabet, "Fuzzy Sliding Mode Method for Speed regulation of a Dual Star Induction Machine Drive fed by Multi-level Inverters," *2018 International Conference on Applied Smart Systems (ICASS)*, pp. 1-7, 2018, https://doi.org/10.1109/ICASS.2018.8651948.

[53] R. Jayaraman, S. Thamizharasan, J. Baskaran, V. Meena, J. Bahadur, V. K. Jadoun, "High-efficiency multilevel inverter topology with minimal switching devices for enhanced power quality and reduced losses," *IET Power Electronics*, vol. 18, no. 1, p. e12851, 2025, https://doi.org/10.1049/pel2.12851.